Spontaneous polyploids and antimutators compete during the evolution of mutator cells

Maxwell A. Tracy, Mitchell B. Lee, Brady L. Hearn, Ian T. Dowsett, Luke C. Thurber, Jason Loo, Anisha M. Loeb, Kent Preston, Miles I. Tuncel, Niloufar Ghodsian, Anna Bode, Thao T. Tang, and Alan J. Herr*

Department of Pathology, University of Washington, Seattle, Washington 98195

* Corresponding author

E-mail: alanherr@uw.edu

Abstract

DNA polymerase (Pol) proofreading and mismatch repair (MMR) defects produce "mutator" phenotypes capable of driving tumorigenesis. "Ultra-mutated" cancers with defects in both pathways exhibit an explosive increase in point mutation burden that appears to reach an upper limit of ~250 mutations/Mb, which may be evidence for negative selection. Simultaneous defects in proofreading and MMR drive error-induced extinction (*EEX*) of haploid yeast. Some yeast mutants escape extinction through antimutator mutations that suppress the mutator phenotype. We report here that other yeast mutants escape by spontaneous polyploidization. We sought to compare these two adaptive strategies during the evolution of haploid and diploid mutators. We first evolved 89 independently isolated haploid mutator strains with mutation rates an order of magnitude below the lethal threshold. Polyploid cells overtook nearly every culture. In a similar manner, we evolved strong diploid mutators, but found only a single tetraploid emerged after ~250 cellular generations. Antimutators dominated these late passage cultures and were present after only 30-40 cellular generations. Whole genome sequencing of independent isolates from the same culture allowed us to construct phylogenetic trees that revealed that a single subclone swept through each culture carrying multiple antimutator mutations affecting the mutator polymerase. Variation in mutation rate between subclones from the same culture suggests some strains carry additional antimutator alleles in other genes. Our findings in diploid mutator yeast suggest that mutator-driven cancer cells may also adapt to the threat of extinction by accumulating multiple antimutator alleles that cooperatively reduce mutation rate to tolerable levels.

Author summary

"Mutator" tumor cells that cannot correct DNA replication errors exhibit an extremely high mutation rate that accelerates their evolution. But this gamble puts them at risk for extinction

due to the accumulation of harmful mutations. Mutator yeast cells escape extinction through "antimutator" mutations that lower mutation rate. We discovered that yeast cells also adapt by duplicating their genome. To understand which adaptation may emerge in mutator-driven tumors, we evolved haploid and diploid mutator yeast cells by long-term propagation. Haploid mutators primarily adapted by genome duplication, thereby protecting themselves from recessive lethal mutations. In contrast, diploid mutators evolved by acquiring multiple antimutator mutations. Our results suggest that mutator-driven tumors may similarly accumulate combinations of mutations that attenuate their high mutation rates.

57 ## Introduction

58 The high fidelity of DNA replication and repair prevents mutations that might otherwise
59 lead to cancer. As first proposed more than 40 years ago, cells with defects in these pathways
60 exhibit an elevated mutation rate ("mutator phenotype") and an accelerated path to malignancy
61 [1,2]. The mutator hypothesis of cancer first gained support from the discovery that Lynch
62 syndrome was caused by defects in mismatch repair (MMR), which normally correct DNA
63 replication errors [3]. Mouse studies later demonstrated that loss of polymerase proofreading
64 also promoted tumorigenesis and strongly synergized with MMR defects [4,5]. More recently,
65 intensive sequencing of cancer genomes revealed that proofreading defects, as well as a wide
66 range of other mutagenic processes, occur in a wide variety of sporadic human tumors [6-10].
67 The most common proofreading-deficient cancers carry heterozygous mutations in *POLE*, which
68 encodes the catalytic subunit of DNA polymerase epsilon (Polε), which acts during leading
69 strand replication [6,10]. Mutations affecting *POLD1*, encoding the lagging strand DNA
70 polymerase (Polδ) catalytic subunit, are also observed [6,10]. Proofreading-deficient tumors
71 frequently carry mutations affecting MMR [6,10]. Far from incidental, in some cases, the MMR
72 defects synergize with proofreading deficiency to ignite a firestorm of mutagenesis [11-13]. In a
73 similar manner, patients with inherited biallelic MMR deficiency frequently develop rapidly
74 mutating tumors with heterozygous mutations affecting the fidelity of Polε or Polδ [14]. Thus,
75 powerful mutator phenotypes based on the synergistic interactions between MMR and
76 proofreading defects represent a reoccurring path in cancer evolution.

77 As an evolutionary strategy, a high mutation rate comes with the risk of error-induced
78 extinction (*EEX*), where every cell in the population eventually acquires a lethal mutation [15].
79 As an extreme manifestation of *EEX*, double mutant haploid yeast spores deficient in Polδ

80 proofreading and MMR cease dividing within 10 cellular generations [16]. Strong mutator
81 phenotypes can also drive *EEX* of diploid yeast, although the maximum tolerated mutation rate
82 (error threshold) is higher than in haploids, consistent with genetic buffering by the diploid
83 genome [17]. Colony formation slows and becomes irregular once mutation rates are within an
84 order of magnitude of the diploid error threshold. Evidence for error thresholds exist in
85 mammals. Mouse embryos completely deficient in both proofreading and MMR initiate
86 development but fail in the second week of gestation [5]. In addition, the proofreading and MMR-
87 deficient tumors mentioned above appear to reach an upper limit of ~ 250 mutations/Mb [14].
88 High mutation loads may inherently restrict cellular longevity. Recent lifespan experiments in
89 yeast demonstrate that strong diploid mutators exhibit a form of genetic anticipation: the longer
90 a lineage exists, the higher the mutation burden, and the shorter the cellular lifespan becomes
91 [18].

92 In the face of *EEX*, a subset of haploid yeast *eex* mutants survive by acquiring
93 "antimutator" mutations that affect the mutator polymerase driving the mutagenesis [15,19] – a
94 mechanism also observed in bacteria [20,21]. However, the majority of *eex* mutants carry
95 mutations that are extragenic to the polymerase gene. Included among these are antimutator
96 mutations affecting the S-phase checkpoint kinase, Dun1, which increase polymerase fidelity by
97 lowering dNTP pool levels [22]. We report here that the most common adaptive event for haploid
98 mutators is spontaneous polyploidization, which buffers cells from the accumulation of
99 mutations. This finding led us to explore how antimutators and spontaneous polyploids compete
100 during evolution of haploid and diploid mutators to understand which pathway might prevail in
101 mutator-driven tumors.

102 **Results**

103 We took a classic yeast genetics approach to identify new extragenic antimutator
104 pathways affecting Polδ and Polε proofreading deficiency (S1A,B Fig). We began with diploid
105 parent strains that were heterozygous for *pol3-01* (Polδ proofreading defective) and deletion of
106 *MSH6 (msh6Δ)* or *pol2-4* (Polε proofreading defective) and *msh2Δ*. After forcing the diploids to
107 undergo meiosis by sporulation [23], we isolated *eex* mutants that suppressed the synthetic
108 growth defects of freshly isolated haploid *pol3-01 msh6Δ* or *pol2-4 msh2Δ* cells. The parental
109 strains were also heterozygous for two distinct transgene insertions at the *CAN1* locus:
110 *CAN1::natMX*, which confers sensitivity to canavanine and resistance to nourseothricin (NTC),
111 and *can1Δ::HIS3*, which confers canavanine resistance and histidine prototrophy. Each *eex*
112 mutant inherited only one of the two *CAN1* alleles, allowing us to cross them to WT haploids with
113 the opposite *CAN1* allele and mating type (haploid yeast cells grow vegetatively as one of two
114 mating-types, *MAT***a** and *MAT*α, which can mate to form *MAT***a**/*MAT*α diploids) and then isolate
115 diploid mapping strains on media that selected for His^+ and NTC-resistant cells. While most of
116 the resulting mapping strains successfully underwent sporulation, the majority failed to produce
117 any viable spores. Several mapping strains with intermediate spore viability produced progeny
118 that carried both *CAN1* alleles. Flow cytometry revealed that these unusual mapping strains
119 were in fact tetraploids (4n) (S1B Fig). The mapping strains with no viable spores were triploids
120 (3n). We inferred that the original *eex* mutants used to make the 3n mapping strains were
121 *MAT***a**/*MAT***a** or *MAT*α/*MAT*α diploids and that the 4n strains were derived from
122 *MAT***a**/*MAT***a**/*MAT***a** or *MAT*α/*MAT*α/*MAT*α triploid *eex* mutants.

123 A bias in how we picked candidate mutants could explain why polyploids were more
124 common than antimutators in our genetic screens. To determine the relative success of these

125 two adaptations in an unbiased manner, we evolved *pol2-4 msh2Δ* cells, which have a mutation
126 rate an order of magnitude below the haploid error threshold [19,24]. We isolated 89
127 independent *pol2-4 msh2Δ* spore clones by dissecting tetrads from *POL2/pol2-4 MSH2/msh2Δ*
128 diploids on growth media that selected for the *URA3* and *LEU2* transgenes tightly linked to the
129 mutator alleles (Fig 1A). Freshly dissected *pol2-4 msh2Δ* haploids form colonies with an uneven
130 perimeter, consistent with the onset of *EEX* and the emergence of *eex* mutant subclones with
131 improved survival. After two days, we isolated four cells from the perimeter of each colony and
132 moved them elsewhere on the plate to assess their colony forming capacity, mutation rate and
133 ploidy (S2A Fig). After removing these cells, we suspended the original colonies in liquid growth
134 media and repeatedly sub-cultured them by diluting the cells 1:500 (~10^5 cells/inoculum) and
135 then growing them to saturation (~10^8 cells), yielding an estimated 10-12 generations per
136 transfer. We assessed ploidy at the initial time point (T1) and then after the 4th (T4) and the 7th
137 transfer (T7).

138 The ploidies of the initial colony suspensions were overwhelming haploid, although 15 out
139 of 89 cultures at this early stage showed evidence of a minor diploid subclone (Fig 1B, S1
140 Dataset). One notable colony suspension (A4) contained both haploid and triploid cells in equal
141 proportions. Two-thirds of the cells isolated from the perimeters of the initial colonies failed to
142 form a second colony — a manifestation of *EEX*. The 120 colonies from viable cells contained
143 12 that were uniformly polyploid (including one triploid (A4.1) from the mixed colony noted above)
144 (S2B Fig, S1 Dataset). To test for antimutators, we measured mutation rates of the haploid
145 subclones that carried the *CAN1::natMX* allele. This involved subcloning these cells a second
146 time to obtain replica colonies. A high frequency of polyploid replica colonies precluded
147 measurements for 12 subclones. Thirteen subclones exhibited the expected mutation rate for

148 *pol2-4 msh2Δ* cells, while twelve subclones displayed an antimutator phenotype (S2C Fig).
149 These results indicate that antimutators and polyploids emerge with similar frequencies during
150 the initial growth of *pol2-4 msh2Δ* haploids and that polyploids continue to arise. Prolonged
151 growth of the original cultures revealed profound fitness differences between these two
152 evolutionary strategies (Fig 1B). At T7 only 2 cultures remained haploid; 10 were mixtures of 1n
153 and 2n cells, and 73 cultures were uniformly 2n or 3n. Thus, polyploids routinely win out over
154 antimutators during the adaptation of haploid cells to the mutator phenotype.

155 In the haploid evolution experiment, cells could have become polyploid by mating or
156 spontaneously [25]. Although deletion of *Homing Endonuclease* (*HO*) stabilizes mating type in
157 our studies, mating-type switching may still occur at a low rate through random DNA breaks at
158 the *MAT* locus, which are then repaired using the transcriptionally silent *HML* (MATα) or *HMR*
159 (MAT**a**) loci [23]. Cross contamination between neighboring wells represents a second potential
160 source of cells of the opposite mating type in our experiment. And although not widely
161 appreciated, same-sex mating can also occur [26]. To determine the relative contributions of
162 mating and spontaneous polyploidization, we isolated a single colony from each evolved culture
163 and performed flow cytometry. Of the 87 isolates, there were 83 diploids, 1 haploid, 1 triploid,
164 and 2 mixed cultures with both 1n and 2n cells (Fig 1C). Mating-type PCR assays revealed 41
165 *MAT***a***/MAT***a**, 36 *MAT*α/*MAT*α and 6 *MAT***a***/MAT*α diploids (Fig 1D). Three of the *MAT***a**/*MAT*α
166 isolates were heterozygous at the *CAN1* locus (*CAN1::natMX/can1Δ::HIS3*) (S2 Dataset),
167 providing clear evidence for rare mating events between cells from neighboring wells. The 3
168 remaining *MAT***a***/MAT*α cells were homozygous for *CAN1::natMX* or *can1Δ::HIS3* and could
169 have arisen through contamination or mating-type switching. Experiments to investigate same-
170 sex mating indicate it occurs at a similar frequency as mating-type switching (Supplementary

171 text S1, S3 Fig). Thus, the predominance of *MAT***a***/MAT***a** or *MAT*α/*MAT*α isolates suggests that
172 the diploids in our evolving populations arise primarily by spontaneous polyploidization.

173 If becoming diploid buffers haploid mutators from deleterious mutation accumulation, then
174 being a tetraploid may confer an additional advantage. To test this idea, we isolated
175 *MAT***a***/MAT***a** and *MAT*α/*MAT*α diploid cells from different evolved cultures by microdissection
176 and mated their daughter cells. We moved the parental diploid cells as well as the resulting
177 tetraploid zygotes to distinct locations on the agar plates to form colonies (Fig 2A). We then
178 mixed each parent diploid strain separately with their tetraploid progeny at different ratios (100:1,
179 10:1, 1:1, 1:10, 1:100) and grew them in competition. The tetraploids overtook the parental
180 diploids in 7 out of 8 competitions, providing strong evidence that tetraploidy buffers these
181 mutator strains from deleterious mutations (Fig 2B). But it is unclear from this experiment
182 whether tetraploids would be similarly favored during the evolution of diploid mutators. The
183 diploid cells used here carry homozygous mutations that arose prior to spontaneous
184 polyploidization, which can only be buffered by mating. Such mutations would be heterozygous
185 from the inception of a strong diploid mutator phenotype.

186 To understand how diploid mutators adapt to the threat of extinction, we again took an
187 evolutionary approach. We first estimated that it would take an *eex* mutant 200 generations to
188 overtake a *pol3-01/pol3-01 msh6Δ/msh6Δ* diploid culture if lethality was driven solely by
189 homozygous inactivation of essential genes [17] (S4 Fig, Dataset 1). We isolated numerous
190 independent *pol3-01/pol3-01 msh6Δ/msh6Δ* zygotes by mating freshly dissected *pol3-01 msh6Δ*
191 haploids (Fig 3A). We evolved 89 clones through ~300 generations, monitoring ploidy at the T1,
192 T10, T19, and T27 transfers (Fig 3B). Only a single pure tetraploid culture emerged at the end
193 of the experiment. To assay for antimutator phenotypes, we isolated independent subclones

194 from T25 *CAN1::natMX/can1Δ::HIS3* cultures, assessed their ploidy, and measured mutation
195 rates. Almost all isolates were diploids (Dataset 1) and exhibited a clear antimutator phenotype.
196 Antimutator subclones also dominated the T13 cultures and were evident as early as T1 (4A
197 Fig). T1 cells from every culture formed variably sized colonies, suggesting that strong selection
198 for *eex* mutants exists by ~30 cellular generations (20 generations/colony and 10 generations
199 for T1) (S5 Fig).

200 Independent T25 isolates from the same *pol3-01/pol3-01 msh6Δ/msh6Δ* culture
201 sometimes displayed different mutation rates (Fig 4B). We wondered whether they shared a
202 common evolutionary history, and therefore sequenced the genomes of eight sets of subclones.
203 In each set, the subclones could be arranged into a phylogenetic tree with ~1300 to 4500 shared
204 mutations in the trunk and ~1400 to 3000 unique mutations in the branches, indicating that a
205 single adapted clone rose to prominence in each culture and then diverged (Fig 4C,D). Thus,
206 differences in mutation rates between subclones likely reflect the presence of additional
207 antimutator mutations in some isolates but not others.

208 The mutations that delineate the phylogenetic trees bear the imprint of the mutator and
209 antimutator phenotypes involved in the evolution of these cultures. We classified the shared
210 and unique mutations according to the 96 trinucleotide contexts defined by the six different
211 mutation subtypes (C:G→A:T, C:G→G:C, C:G→T:A, T:A→A:T, T:A→C:G, T:A→G:C), flanked
212 by all possible 5' and 3' nucleotides. We then compared the mutation spectra, within and
213 between strains, by the hypergeometric test [27]. The spectra of the trunk mutations were largely
214 the same between different cultures, consistent with each culture beginning with a common
215 mutator phenotype (Fig 4D, S6 Fig, S2 Dataset). The spectrum of unique mutations in each
216 branch of a given tree differed substantially from that of the trunk mutations ($p < 0.0001$),

217 although generally not from each other, consistent with the antimutator phenotype arising prior
218 to their divergence (Fig 4D, S6 Fig). Particularly sharp decreases in the relative abundance of
219 C:G→A:T mutations were observed in the branches of all trees. Despite these similarities, the
220 spectra of unique mutations from different evolved cultures were often statistically different from
221 each other, suggesting that the antimutator alleles altered replication fidelity in distinct ways (Fig
222 4D, S2 Dataset). Thus, acquisition of an antimutator phenotype coincides with the key adaptive
223 event in each culture and fundamentally changes the mutation spectra.

224 To understand how the cells attenuated the mutator phenotype, we annotated the
225 mutations (S2 Dataset) and compared the affected genes. All 8 strain sets acquired multiple
226 *pol3* mutations prior to their divergence (Fig 4C,D). Many mutations affect the same amino acid
227 residue or are identical to known antimutator mutations (*A704V(2x), A786V*, *A677T, D831A,*
228 *R475S, R815C*) [15,17,28]. Polδ plays an essential role in DNA replication. Both *pol3-01* alleles
229 contribute to error-induced extinction in these cells, but only one allele needs to remain functional
230 for cells to survive. Thus, the premature nonsense codons observed in three trees (B1, C2, D2)
231 effectively function as antimutator alleles by inactivating one of the two *pol3-01* alleles. The
232 remaining missense mutations affecting *pol3-01* may similarly inactivate polymerase function or
233 may be *bona fide* antimutator alleles that have not previously been identified. Candidate
234 antimutators include *P942L* and *M578I*, which were observed in two independent lineages, and
235 mutations affecting P796, which were isolated three independent times (*P796L*(2x) and *P796S*)
236 — once in combination with a stop codon.

237 To test the hypothesis that *pol3* mutations are under positive selection, we compared the
238 ratio of nonsynonymous and synonymous mutations (dN/dS) across the genome using *dNdscv*,
239 an R-program which normalizes the observed dN/dS ratio by the 192-trinucleotide mutation

240 spectra of each gene before assessing whether the observed ratio departs from neutrality
241 (dN/dS = 1) [29]. We analyzed the mutations from the trunks of the 8 lineages and found that
242 only *pol3* mutations are under positive selection (q = 0.004, corrected *p*-value using Benjamini
243 and Hochberg's false discovery rate). Mutations in other genes, within the resolution of this
244 dataset, accumulate in a neutral fashion. The genome-wide dN/dS ratio for the trunk mutations
245 was 1.0, as was the dN/dS ratios for subclasses of trunk mutations involving missense or
246 nonsense mutations (Fig 4E). Repeating this analysis for the 23 unique sets of mutations from
247 the branches failed to reveal any other genes under strong selection after adaption. Intriguingly,
248 the genome-wide dN/dS ratio for nonsense mutations was 0.8, indicating that negative selection
249 begins to act against the most deleterious class of mutations during extended propagation of
250 these lines. When the mutations found in trunk and branches are combined, evidence for
251 negative selection remains, but *pol3* mutations do not emerge from the multiple testing correction
252 as significant. Thus, the identification of antimutator mutations by *dNdscv* during the evolution
253 of mutator-driven tumors may be masked without phylogenic information.

254 Discussion

255 Cell lineages with ultra-mutator phenotypes face a progressive loss of fitness and even
256 extinction unless they adapt by becoming polyploid or acquiring antimutator mutations. The
257 competition between polyploids and antimutators during the evolution of mutators is influenced
258 by the rate at which they arise and the extent to which they preserve or even enhance fitness.
259 In our study of *pol2-4 msh2Δ* haploids, we found that two-thirds of cells sampled from the
260 perimeter of the initial colonies (<20 cellular generations) were inviable, illustrating the strong
261 selection pressure for *eex* mutants. At this early stage, polyploids and antimutators were present
262 with similar frequencies. The rate of spontaneous polyploidization of haploid yeast was recently

263 estimated at 7 x 10^{-5} per division [30], which is similar to the rate of *CAN1* inactivation in *pol2-4*
264 *msh2Δ* cells (1-2 x 10^{-4}). The overwhelming success of polyploids over antimutators during the
265 evolution of *pol2-4 msh2Δ* cultures supports a model in which they emerge based on their ability
266 to buffer the genome from deleterious mutations, as previously observed with chemically
267 mutagenized haploids [31]. Spontaneous diploids have risen to prominence in previous WT
268 haploid evolution studies over longer time scales [32-34]. The efficiency at which this occurs
269 varies, and may depend on the nature of the strain, the culture conditions, and the presence of
270 preexisting diploids within the initial population. Two different studies place the increase in
271 fitness of diploids over WT haploids at around 3.5% per generation [33,34]. With strong
272 mutators, the fitness differential between spontaneous polyploids and haploid cells is likely much
273 larger and constantly increasing as mutations accumulate within haploid genomes. And
274 conceivably, since the mutator phenotype continues unabated after polyploidization, fitness-
275 enhancing mutations may arise that in some cases accelerate the selective sweep.

276 Despite being buffered from deleterious mutations, diploids clearly lose fitness as
277 mutations accumulate. The variable growth of *pol3-01/pol3-01 msh6Δ/msh6Δ* T1 colonies
278 indicates that by 30-40 cellular generations there exists strong selection pressure for *eex*
279 mutants to emerge. The rate of tetraploidization of diploid yeast is unknown, but it may be
280 comparable to the diploidization of haploids. The *pol3-01/pol3-01 msh6Δ/msh6Δ* cells exhibit a
281 five- to ten-fold higher mutation rate than *pol2-4 msh2Δ* haploids. Together, these two
282 observations would seem to favor the emergence of antimutators over polyploids. However,
283 mutator suppression requires at least two independent *pol3* mutations, whereas only a single
284 event is required for polyploidization. Part of the success of diploid antimutators may stem from
285 the fact that they are already buffered from deleterious mutations. Moreover, heterozygous

286 antimutator mutations may provide incremental protection from extinction, giving time for
287 additional antimutator mutations to occur that give more complete protection. Evidence
288 suggests that tetraploids may be inherently less fit than diploids [32]. Tetraploids are known to
289 suffer higher rates of genomic instability and depend more heavily on factors involved in
290 homologous recombination [35]. In the context of a mutator phenotype, a higher rate of
291 homologous recombination in tetraploids would limit buffering of deleterious mutations by
292 promoting loss of heterozygosity.

293 The ease with which diploid yeast mutator cells adapt to the risk of error-induced
294 extinction suggests that similar events may occur during the evolution of mutator-driven cancers.
295 The simplest antimutator change available to tumors that carry a heterozygous *POLE* allele is
296 simply to inactivate or suppress the mutator allele. But other changes that attenuate the mutator
297 phenotype may also be possible. Recent evolution studies in diploid yeast pointed to
298 unconventional mutator phenotypes caused by heterozygous mutations in house-keeping genes
299 [36]. If mutation rate can be enhanced by such mutations, perhaps it may be attenuated as
300 well. While our dN/dS analysis only found evidence for selection acting on the *POL3* gene, we
301 observed variation in mutation rate within the same phylogenic tree suggesting that other
302 antimutator mutations exist within the thousands of mutations present within these genomes.
303 The vast phenotypic space created by combinations of heterozygous mutations may be critical
304 to understanding the evolution of mutation rate in diploids.

305 ## Materials and Methods

306 **Culture conditions.** Yeast propagation and tetrad dissection followed standard
307 procedures [37]. Unless otherwise noted, reagents were purchased from Fisher Scientific or
308 Sigma. For rich liquid media, we used YPD (1% wt/vol yeast extract, 2% wt/vol peptone, 2%

309 wt/vol dextrose). For rich solid media we used YPD or synthetic complete (SC) [6.7 g Difco
310 yeast nitrogen base without amino acids, 2% wt/vol dextrose, 2 g/L SC amino acid Mix (SCM)
311 (Bufferad)] supplemented with 2% wt/vol agar. For drop-out media, SCM powders lacking
312 specified amino acids were either purchased from Bufferad or made to the same specifications
313 [38]. For haploid mutation rates, we used SC plates lacking arginine (SC-Arg) with 60 μg/mL
314 canavanine (Can). For mutation rates with diploid strains we used SC_MSG-Arg [1.7 g Difco
315 yeast nitrogen base without amino acids or ammonium sulfate, 1 g/L monosodium glutamate
316 (for a nitrogen source), 2% wt/vol dextrose, 2 g/L SCM-arginine)] with 60 μg/mL Can and 100
317 μg/mL nourseothricin (NTC) [17]. We used similar plates lacking histidine and containing NTC
318 (SC_MSG-His+NTC) to select for mating between *CAN1::natMX* and *can1Δ::HIS3* cells (see
319 below).

320 **Yeast strains.** The diploid parent strain used for these experiments, AH0401, is a
321 BY4743 derivative engineered to be heterozygous at the *CAN1* locus [17]. One allele carries the
322 *natMX* transgene (encoding resistance to the drug NTC) inserted just downstream of the *CAN1*
323 coding sequence (*CAN1::natMX*), while the other *CAN1* allele is deleted and replaced with *HIS3*
324 (*can1Δ::HIS3*). Selection for *can1* mutants in the presence of canavanine and NTC allows us to
325 score *bona fide can1* mutants without the high background of *can1Δ::HIS3/can1Δ::HIS3* mitotic
326 recombinants [17]. The four WT strains used for generating mapping strains (S1 Fig) and for
327 the same-sex mating experiments (S3 Fig) were dissected from the same AH0401 tetrad:
328 AH4002 (*MAT*α *CAN1::natMX)*, AH4003 (*MAT***a** *CAN1::natMX)*, AH4010 (*MAT*α *can1Δ::HIS3*),
329 and AH4015 (*MAT***a** *can1Δ::HIS3*). AH12721 is a *POL2/URA3::pol2-4 MSH2/msh2Δ::LEU2*
330 strain isolated by mating freshly dissected spores from AH2801 (*POL2/URA3::pol2-4*
331 *MSH6/msh6Δ::LEU2*) [39] and AH5610 (*MSH2/msh2Δ::LEU2*). Zygotes were isolated by

332 microdissection after 8 hours and allowed to form colonies, which were then genotyped. AH5610
333 was constructed for this study by transforming AH0401 with a *LEU2* PCR product amplified from
334 pRS416 with Msh2U and Msh2D [19]. AH2601 is a previously described *POL3/URA3::pol3-01*
335 *MSH6/msh6Δ::LEU2* strain [18]. All strains derived from mating between *pol3-01 msh6Δ* spores
336 used in the evolution experiment were designated AH164_NN, where "NN" refers to their
337 coordinate in the 96-well plate.

338 **Isolation of eex mutants.** The *pol2-4 msh2Δ eex* mutants (S1 Fig) were obtained by
339 dissecting AH12721 spores on SC-Leu-Ura plates and then re-plating the resulting slow-growing
340 colonies for faster growing mutants. We employed a different strategy for *pol3-01 msh6Δ eex*
341 mutants. Since these double mutant haploids form only microcolonies, we plated a large
342 preparation of random spores onto SC-Ura-Leu media and picked viable colonies. To isolate
343 mapping strains, we mated each *eex* mutant in parallel with AH4002, AH4003, AH4010, and
344 AH4015 and plated the mutants on SC_MSG-His+NTC. Candidates that only mated with one
345 of the four strains were carried forward for genetic analyses.

346 **Same-sex matings.** Same-sex matings (S3 Fig) were performed by mixing ~5 x 10^6 cells
347 of two strains with the same mating type but opposite *CAN1* alleles (*can1Δ::HIS3* and
348 *CAN1::natMX*) in a microtiter plate with YPD and incubating at 30°C for 8 hours without shaking.
349 *CAN1::natMX/can1Δ::HIS3* diploids were then selected on SC_MSG-His+NTC media. Mating
350 type PCRs were performed as described [30].

351 **Evolution experiments.** To obtain *URA3::pol2-4 msh2Δ::LEU2* double mutant spores
352 we dissected tetrads on SC-Ura-Leu. After two days of growth, we isolated single cells from the
353 perimeter of each colony by microdissection and moved them below the colony to form new

354 colonies (S2*A* Fig). We then suspended the main colonies in 100 µls of H_2O in 96-well format
355 (Fig 1). Random empty wells were interspersed among the samples to monitor for
356 contamination. We made glycerol stocks from part of the cell suspension. From the remaining
357 cell suspensions, we diluted the cells 1:50 in YPD, and grew 3 hours before removing aliquots
358 for the first flow cytometry measurement after which the cultures were grown to saturation and
359 then subcloned as described below.

360 To isolate *URA3::pol3-01/URA3::pol3-01 msh6Δ::LEU2/msh6Δ::LEU2* diploids, AH2601
361 tetrads were dissected on SC-Ura-Leu plates and spores were separated from each other by
362 ~100 µm (the width of two diameters of the dissecting needle). After 2 to 3 divisions, prototrophic
363 cells from different tetrads were placed next to each other to allow mating. Half of the pairings
364 produced zygotes after 2 to 3 additional divisions. Zygotes were moved to a defined coordinate
365 on the plate and allowed to form a colony. Colonies were picked from the plate and suspended
366 in 100 µls of H_2O. We used 30 µls of the cell suspensions to inoculate 500 µls cultures, 40 µls
367 for glycerol stocks, and the remaining cell suspension to measure mutation rates (see below).

368 In both evolution experiments, the strains were propagated at 30°C with constant shaking
369 in sterile Nunc 96 deep-well storage blocks (Thermo Scientific, 260252), covered with an
370 AeraSeal (Excel Scientific) gas-permeable disposable plate sealer. Each well had 500 µls of
371 YPD and a single 3 mm glass bead to maintain cells in suspension. Sub-culturing steps were
372 performed by transferring 1 ul volumes from saturated cultures to 500 µls of fresh YPD using an
373 8-channel pipettor. Frozen -80°C glycerol stocks of the cultures were made every three transfers
374 in 96-well format. To recover cultures from storage, the plates were first thawed at room
375 temperature and then 5 µls were transferred into 250 µl of fresh media.

376 **Mutation rates.** Mutation rates by fluctuation analysis were performed essentially as
377 described [17]. To determine the mutation rate of the zygote colonies, 10 µls of the original
378 suspension (see above) were spot-plated directly on SC_MSG-Arg+CAN+NTC plates. Another
379 10 µls were used for 10-fold serial dilutions. With each dilution, 10 µls were plated on the
380 mutation rate plate and 10 µls on SC media to estimate the total number cells in each colony
381 (Nt). Only half of the zygote colonies had the *CAN1::natMX/can1Δ::HIS3* genotype suitable for
382 mutation rate measurements. Thirty colonies with similar Nt values were used as "replica
383 colonies" to estimate the average number of mutational events (*m*) by maximum likelihood using
384 newton.LD.plating in the R package rSalvador [40]. LD.plating was used to calculate confidence
385 intervals. For mutation rates of all subclonal isolates (Fig 4A, S2 Fig), replica colonies were
386 obtained by plating serial dilutions onto SC media. For mutation rate calculations we typically
387 used mutation counts from 8 replica colonies. In some assays of T1 subclones in Fig 4A, 1 or 2
388 replica colonies had very low mutation counts (0 or 1 mutants vs 100's). These clear outliers
389 were censored under the assumption that they represented an antimutator or polyploid subclone.
390 Cohorts with more than 2 such outliers were censored completely.

391 **Flow cytometry.** Overnight cultures were diluted 1:50 in fresh YPD and grown for 3-5
392 hours. 100 µls of cells were recovered by centrifugation and washed twice in an equal volume
393 of water by resuspending them and centrifuging again. We then resuspended the cells in 70%
394 ethanol and incubated them at least 1 hour at room temperature or overnight at 4°C. We
395 recovered the cells again by centrifugation, washed once with water, and then resuspended
396 them in 50 mM sodium citrate with RNaseA (10 µg/mL). The cells were heated to 95°C for 15
397 minutes and then incubated for 3 to 4 hours at 37°C. The cells were recovered by centrifugation
398 and resuspended at a concentration of 10^6 cells/mL in 50 mM sodium citrate with 2 µM Sytox

399 Green (Life Technologies). After 1 hour at room temperature, the cells were sonicated for 30
400 seconds with 1 second pulses in a Misonix cup horn sonicator and then analyzed on a BD Accuri
401 c6 flow cytometer using the FL1 detector. Plots in S1 Dataset are organized in the 96 well-
402 format used for each experiment. Histogram plots of the data were generated using the c6
403 software, which allows multiple plots to be overlaid. Plots used as controls are indicated at the
404 top of each experiment.

405 **Genome sequencing and analysis.** We performed whole genome sequencing of
406 subclones from the AH164 evolved cultures as described [18] except that we used a variant
407 frequency cutoff of 0.1 for SNPs to demonstrate that the sequenced genomes were indeed from
408 2n and not 4n cells (S2 Dataset). We used a variant frequency cutoff of 0.3 for indels to minimize
409 false positives at repetitive sequences due to frameshift errors during library preparation. We
410 wrote a python script to compare subclones from the same culture and create lists of shared and
411 unique mutations found in each strain. The program only assesses positions in the genome with
412 18-fold depth coverage in all subclones (S2 Dataset). We annotated the SNP lists using
413 Annotate 0.1 [41] and the Indel lists with a modified version of the program that reports the 3'
414 peptide produced by the frameshift. We used the SNP lists to determine the 96-trinucleoide
415 mutation spectra using snv-spectrum (https://github.com/aroth85/snv-spectrum). We wrote a
416 python script which creates a 2 x 96 table of the output of snv-spectrum for two different variant
417 lists and then computes a Monte Carlo estimation of the *p*-value of the hypergeometric test [27],
418 under the null hypothesis that they came from the same population (S1 File). Implementation of
419 the test involves construction of 10,000 random tables that maintain the same row and column
420 totals [42] and then calculation of the hypergeometric probability of each table. The *p*-value
421 represents the number of random tables whose hypergeometric probability is less than the

422 observed. The conservative Bonferroni multiple testing correction was used to estimate the *p*-
423 value cut-off for significance for each set of comparisons (S2 Dataset). Finally, we used the
424 SNP lists described above to determine the dN/dS ratios of individual genes and of the entire
425 genome using the R-package *dNdscv* [29].

426 **Acknowledgements**

427 We thank Dr. Maitreya Dunham for use of a flow cytometer and horn sonicator. We also
428 thank Drs. Dunham and Scott Kennedy for critically reading the manuscript.

429 ## References Cited

430 1. Loeb LA, Springgate CF, Battula N (1974) Errors in DNA replication as a basis of malignant
431 changes. Cancer Res 34: 2311-2321.
432 2. Loeb LA (2016) Human Cancers Express a Mutator Phenotype: Hypothesis, Origin, and
433 Consequences. Cancer Res 76: 2057-2059.
434 3. Lynch HT, Lynch PM, Lanspa SJ, Snyder CL, Lynch JF, et al. (2009) Review of the Lynch
435 syndrome: history, molecular genetics, screening, differential diagnosis, and medicolegal
436 ramifications. Clin Genet 76: 1-18.
437 4. Goldsby RE, Lawrence NA, Hays LE, Olmsted EA, Chen X, et al. (2001) Defective DNA
438 polymerase-δ proofreading causes cancer susceptibility in mice. Nat Med 7: 638-639.
439 5. Albertson TM, Ogawa M, Bugni JM, Hays LE, Chen Y, et al. (2009) DNA polymerase ε and δ
440 proofreading suppress discrete mutator and cancer phenotypes in mice. Proc Natl Acad Sci U S
441 A 106: 17101-17104.
442 6. Network CGA (2012) Comprehensive molecular characterization of human colon and rectal
443 cancer. Nature 487: 330-337.
444 7. Palles C, Cazier JB, Howarth KM, Domingo E, Jones AM, et al. (2012) Germline mutations
445 affecting the proofreading domains of POLE and POLD1 predispose to colorectal adenomas and
446 carcinomas. Nat Genet 45: 136-144.
447 8. Church DN, Briggs SEW, Palles C, Domingo E, Kearsey SJ, et al. (2013) DNA polymerase ε and
448 δ exonuclease domain mutations in endometrial cancer. Hum Mol Genet 22: 2820-2828.
449 9. Yoshida R, Miyashita K, Inoue M, Shimamoto A, Yan Z, et al. (2011) Concurrent genetic
450 alterations in DNA polymerase proofreading and mismatch repair in human colorectal cancer. Eur
451 J Hum Genet 19: 320-325.
452 10. Kandoth C, Schultz N, Cherniack AD, Akbani R, Liu Y, et al. (2013) Integrated genomic
453 characterization of endometrial carcinoma. Nature 497: 67-73.
454 11. Campbell BB, Light N, Fabrizio D, Zatzman M, Fuligni F, et al. (2017) Comprehensive Analysis of
455 Hypermutation in Human Cancer. Cell 171: 1042-1056.e1010.
456 12. Hodel KP, de Borja R, Henninger EE, Campbell BB, Ungerleider N, et al. (2018) Explosive
457 mutation accumulation triggered by heterozygous human Pol ε proofreading-deficiency is driven
458 by suppression of mismatch repair. eLife 7: e32692.
459 13. Haradhvala NJ, Kim J, Maruvka YE, Polak P, Rosebrock D, et al. (2018) Distinct mutational
460 signatures characterize concurrent loss of polymerase proofreading and mismatch repair. Nat
461 Commun 9: 1746.
462 14. Shlien A, Campbell BB, de Borja R, Alexandrov LB, Merico D, et al. (2015) Combined hereditary
463 and somatic mutations of replication error repair genes result in rapid onset of ultra-hypermutated
464 cancers. Nat Genet.
465 15. Herr AJ, Ogawa M, Lawrence NA, Williams LN, Eggington JM, et al. (2011) Mutator suppression
466 and escape from replication error–induced extinction in yeast. PLoS Genet 7: e1002282.
467 16. Morrison A, Johnson AL, Johnston LH, Sugino A (1993) Pathway correcting DNA replication
468 errors in *Saccharomyces cerevisiae*. EMBO J 12: 1467-1473.
469 17. Herr AJ, Kennedy SR, Knowels GM, Schultz EM, Preston BD (2014) DNA replication error-
470 induced extinction of diploid yeast. Genetics 196: 677-691.
471 18. Lee MB, Dowsett IT, Carr DT, Wasko BM, Stanton SG, et al. (2019) Defining the impact of
472 mutation accumulation on replicative lifespan in yeast using cancer-associated mutator
473 phenotypes. Proc Natl Acad Sci USA 116: 3062-3071.
474 19. Williams LN, Herr AJ, Preston BD (2013) Emergence of DNA polymerase ε antimutators that
475 escape error-Induced extinction in yeast. Genetics 193: 751-770.
476 20. Fijalkowska IJ, Schaaper RM (1995) Effects of *Escherichia coli dnaE* antimutator alleles in a
477 proofreading-deficient *mutD5* strain. J Bacteriol 177: 5979-5986.

21. Reha-Krantz LJ (1988) Amino acid changes coded by bacteriophage T4 DNA polymerase mutator mutants. Relating structure to function. J Mol Biol 202: 711-724.
22. Williams LN, Marjavaara L, Knowels GM, Schultz EM, Fox EJ, et al. (2015) dNTP pool levels modulate mutator phenotypes of error-prone DNA polymerase ε variants. Proc Natl Acad Sci U S A.
23. Haber JE (2012) Mating-type genes and MAT switching in Saccharomyces cerevisiae. Genetics 191: 33-64.
24. Herr AJ, Williams LN, Preston BD (2011) Antimutator variants of DNA polymerases. Crit Rev Biochem Mol Biol 46: 548-570.
25. Ganem NJ, Storchova Z, Pellman D (2007) Tetraploidy, aneuploidy and cancer. Curr Opin Genet Dev 17: 157-162.
26. Strathern J, Hicks J, Herskowitz I (1981) Control of cell type in yeast by the mating type locus: The α1-α2 hypothesis. J Mol Biol 147: 357-372.
27. Adams WT, Skopek TR (1987) Statistical test for the comparison of samples from mutational spectra. J Mol Biol 194: 391-396.
28. Dennis DG, McKay-Fleisch J, Eitzen K, Dowsett I, Kennedy SR, et al. (2017) Normally lethal amino acid substitutions suppress an ultramutator DNA Polymerase δ variant. Sci Rep 7: 46535.
29. Martincorena I, Raine KM, Gerstung M, Dawson KJ, Haase K, et al. (2017) Universal Patterns of Selection in Cancer and Somatic Tissues. Cell 171: 1029-1041.e1021.
30. Harari Y, Ram Y, Rappoport N, Hadany L, Kupiec M (2018) Spontaneous Changes in Ploidy Are Common in Yeast. Curr Biol 28: 825-835 e824.
31. Mable BK, Otto SP (2001) Masking and purging mutations following EMS treatment in haploid, diploid and tetraploid yeast (Saccharomyces cerevisiae). Genet Res 77: 9-26.
32. Gerstein AC, Chun HJ, Grant A, Otto SP (2006) Genomic convergence toward diploidy in Saccharomyces cerevisiae. PLoS Genet 2: e145.
33. Venkataram S, Dunn B, Li Y, Agarwala A, Chang J, et al. (2016) Development of a Comprehensive Genotype-to-Fitness Map of Adaptation-Driving Mutations in Yeast. Cell 166: 1585-1596.e1522.
34. Fisher KJ, Buskirk SW, Vignogna RC, Marad DA, Lang GI (2018) Adaptive genome duplication affects patterns of molecular evolution in Saccharomyces cerevisiae. PLoS Genetics 14: e1007396.
35. Storchova Z, Breneman A, Cande J, Dunn J, Burbank K, et al. (2006) Genome-wide genetic analysis of polyploidy in yeast. Nature 443: 541-547.
36. Coelho MC, Pinto RM, Murray AW (2019) Heterozygous mutations cause genetic instability in a yeast model of cancer evolution. Nature 566: 275-278.
37. Sherman F (2002) Getting started with yeast. In: Guthrie C, Fink GR, editors. Part B: Guide to Yeast Genetics and Molecular and Cell Biology. Volume 350 ed. San Diego: Academic Press. pp. 3-41.
38. Kaiser C, Michaelis, S., Mitchell, A. (1994) Methods in Yeast Genetics: A Laboratory Course Manual: Cold Spring Harbor Laboratory Press. 202 p.
39. Kennedy SR, Schultz EM, Chappell TM, Kohrn B, Knowels GM, et al. (2015) Volatility of Mutator Phenotypes at Single Cell Resolution. PLoS Genet 11: e1005151.
40. Zheng Q (2015) A new practical guide to the Luria–Delbrück protocol. Mutat Res Fund Mol Mech Mutagen 781: 7-13.
41. Pashkova N, Gakhar L, Winistorfer SC, Sunshine AB, Rich M, et al. (2013) The yeast Alix homolog Bro1 functions as a ubiquitin receptor for protein sorting into multivesicular endosomes. Dev Cell 25: 520-533.
42. Agresti A, Wackerly D, Boyett JM (1979) Exact conditional tests for cross-classifications: approximation of attained significance levels. Psychometrika 44: 75-83.

528 ## Figure Legends

529 **Fig 1. Spontaneous polyploids routinely emerge during the evolution of *pol2-4 msh2Δ***
530 **haploids.** (A) Isolation of *pol2-4 msh2Δ* haploids from sporulated parental diploid cells (2n).
531 Diploid genotype indicated to the right. Arrows, from left to right, indicate manipulations of
532 cells: sporulation, tetrad dissection, and inoculation into 96-well culture blocks. Following
533 tetrad dissection, double mutant *pol2-4 msh2Δ* spores (blue cells) selectively form colonies on
534 media lacking uracil and leucine (green box). (B) Evolution of *pol2-4 msh2Δ* mutators.
535 Independent isolates were cultured in 96-well format by diluting 1:500 with each transfer (T).
536 Ploidy was assessed by flow cytometry at T1, T4, and T7 (S1 for histograms). Color of boxes
537 indicate the ploidy or mixture of ploidies of each culture (see top for key). (C) Ploidy of single
538 cell subclones isolated from T7. (D) Mating-type of single cell subclones. *Top*, Schematic of
539 *MAT***a** and *MAT*α mating type loci, PCR primers (arrows), and expected DNA sizes. *Bottom*,
540 PCR products run on 2% agarose gels, labeled by their coordinates in the 96-well block; *-ve*,
541 negative (no cells) controls; *cn,* culture censored during evolution. The 500bp fragment of the
542 Invitrogen 1kb plus ladder is indicated to the left.

543 **Fig 2. Competition between diploid mutator parents and tetraploid offspring.** (A)
544 Experimental design. *MAT*α/*MAT*α and *MAT***a**/*MAT***a** subclones from the *pol2-4 msh2Δ*
545 evolved cultures (see Fig 1B) were mated. Cell suspensions of the resulting tetraploid and
546 parental diploid colonies were counted, mixed then competed through 8 serial transfers. (B)
547 Ploidy measurements after the first (T1) and eighth (T8) serial transfers. Letter and numbers
548 to the left indicate location in the 96 well culture block described in Fig 1. Color of boxes
549 indicate the ploidy or mixture of ploidies of each culture (see top).

550 **Fig 3. Strong diploid mutators maintain diploidy during evolution.** (A) Isolation of *pol3-*
551 *01/pol3-01 msh6Δ/msh6Δ* zygotes. *Top,* Double mutant *pol3-01 msh6Δ* haploids, identified by
552 dissecting tetrads on selective media (Sc-Ura-Leu), were mated to form zygotes. Zygotes
553 were then moved to new locations on the plate to form colonies. *Bottom,* Growth phenotypes
554 of the initial zygote colonies. Colonies were picked from left to right. Those used for evolution
555 are indicated by either their 96-well coordinate or a dash (-). Colonies without a label or dash
556 were not evolved. (B) Ploidy of evolved cultures after one (T1), ten (T10), nineteen (T19), and
557 twenty-seven (T27) serial transfers. Color of boxes indicate the ploidy or mixture of ploidies of
558 each culture as depicted in the key at the top.

559 **Fig 4. Strong diploid mutators adapt through antimutator alleles.** (A) Mutation rates of *pol3-*
560 *01/pol3-01 msh6Δ/msh6Δ* subclones. Single cell subclones were isolated after the first (T1),
561 thirteenth (T13), and twenty-fifth (T25) transfers. Mutation rates were determined by a
562 canavanine resistance (Can^R) fluctuation assay (see Dataset 1 for mutation rates and 95%
563 confidence intervals). (B) Variation in mutation rates depicted of T25 subclones from the same
564 culture. Alternating shades of red indicate groups of subclones. (C) Phylogenetic trees of above
565 subclones based on whole genome sequencing. Observed *pol3* mutations are in blue lettering
566 (bold represents known or likely antimutators). (D) Representative mutation spectra of shared
567 (trunk) and unique mutations (see S6 Fig for mutation spectra of all trees). Each mutation site
568 (represented here by the pyrimidine base T or C) was categorized into one of the 96 mutation
569 types created by subdividing the 6 general mutation types (C→A, C→G, C→T, T→A, T→C,
570 T→G) into the 16 possible tri-nucleotide contexts (see boxes to the lower right for contexts; blue,
571 black, and red bars correspond to mutation sites involving C; gray, green and pink bars
572 correspond to mutation sites involving T). Bar height corresponds to the fraction each mutation

573 type represents of the total mutations (given in the right-hand corner of each plot). Inset table:
574 *p*-values of the hypergeometric test of similarity between mutation spectra. (E) Genome-wide
575 dN/dS ratios of trunk and branch mutations.

576

577 ## Supporting Information

578 **S1 Text. Same sex mating.** Here, we describe experiments performed to investigate the
579 contribution of same-sex mating to polyploid formation.

580 **S1 Fig. Discovery of spontaneous polyploid *eex* mutants.** (A) Synthetic growth phenotypes
581 of freshly dissected pol3-01 msh6Δ and pol2-4 msh2Δ spore clones. Top, Schematic of strain
582 genotypes and tetrad dissections. Bottom, Images of tetrad dissections after 48 hours of growth.
583 Colored circles indicate genotypes. (B) Isolation of eex mutants and evidence for
584 polyploidization. Top, Scheme for isolating eex mutants and the generation of mapping strains.
585 Bottom, Flow cytometry traces of two representative polyploid strains (AH13214 and AH13238;
586 see S1 Dataset) and 1n, 2n, and 4n controls as well as tally of the ploidies of the mapping strains.

587 **S2 Fig. Polyploids and antimutator subclones emerge with similar frequencies during the**
588 **evolution of *pol2-4 msh2Δ* cultures.** (A) Representative images of colonies. Clockwise from
589 the top left: initial colonies after 24 hours, A4 (a mixture of 1n and 3n cells) is circled in yellow;
590 close-up of A4 just after removing single cells from the perimeter (holes were punched into the
591 agar to mark origin of cells 1 through 4); colony forming capacity of single cells (A4.1 is circled
592 in yellow). (B) Ploidy of colonies derived from single-cell clones (see S1 Dataset for histograms),
593 named for the coordinate of the parent strain in the evolved 96-well plate and the isolate number.
594 (C) Mutation rate measurements of haploid cultures as determined by fluctuation analysis of
595 canavanine resistance (Can^R). Error bars represent 95% confidence intervals. (See S1 Dataset
596 for Table of values.)

597 **S3 Fig. Test for same-sex mating between mutator cells.** (A) Experimental design. Same
598 sex haploid cultures with opposite CAN1 alleles (*CAN1::natMX*, *can1Δ::HIS3*) were mixed and

599 plated for *CAN1::natMX/can1Δ::HIS3* diploids. (B) Summary of flow cytometry and mating-type
600 PCR assays of colonies resulting from the crosses indicated in the white boxes. The mutator
601 cultures used for each cross are indicated by their 96-well coordinate (see Fig 1). The color of
602 the box indicates ploidy (see S1 Dataset for individual histograms). Results of Mating type PCR:
603 **α**, MATα; **a**, MATa (C) Mating-type PCR gels.

604 **S4 Fig. Simulation of eex adaption during diploid mutator evolution.** Exponential growth
605 of *pol3-01/pol3-01 msh6Δ/msh6Δ* cells (Mutator, red line) and an eex mutant (blue line) with a
606 10-fold lower mutation rate were modeled assuming the only limiting factor for growth was
607 homozygous inactivation of essential genes (see S1 Dataset). Each peak models a 1:500
608 dilution of the culture from ~10^8 cells to ~10^5 cells.

609 **S5 Fig. Colony forming capacity of evolved *pol3-01/pol3-01 msh6Δ/msh6Δ* cultures.** Ten-
610 fold serial dilutions from overnight cultures were plated on SC plates and incubated for two days
611 at 30°C. T1 and T13 refer to first and thirteenth sub-culturing steps after the initial inoculations.
612 The culture designation on the left refers to the position of the culture in the 96 well plate (see
613 Fig 3).

614 **S6 Fig. Mutation spectra and phylogenetic relationships of evolved *pol3-01/pol3-01*
615 *msh6Δ/msh6Δ* T25 subclones.** Mutational variants identified by whole genome sequencing of
616 subclones isolated from different evolved cultures were classified as shared (trunk) and unique.
617 The nucleotide context 5' and 3' of each mutational site (represented as the pyrimidine base T
618 or C) were used to classify the 6 mutation types (C:G→A:T, C:G→G:C, C:G→T:A, T:A→A:T,
619 T:A→C:G, T:A→G:C) into 96 trinucleotide contexts. Each mutation type family is color-coded
620 (see Key for color and context order). The bar height for mutation type represents the fraction

621 of the total mutations (to the right of each plot). Phylogenetic trees: line length corresponds to
622 the number of mutations, line color corresponds to mutation spectra, observed pol3 mutations
623 are in blue lettering (bold represents known or likely antimutators). Inset tables: *p*-values
624 determined by the hypergeometric test.

625 **S1 File. Hypergeometric test.** Markdown of the python 3 script for the hypergeometric test of
626 similarity between mutation spectra.

S1 Dataset. Flow cytometry, mutation rates, and modeling of diploid evolution.

Page	***Description***
1	Ploidy measurements of *eex* mapping strains described in S1B Fig.
2	Ploidy measurements of *pol2-4 msh6*Δ evolved cultures described in Fig 1B.
3	Ploidy measurements of *pol2-4 msh6Δ* T8 subclones described in Fig 1C.
4	Ploidy measurements of *pol2-4 msh6Δ* subclones described in S2A Fig.
5	Mutation rate measurements of *pol2-4 msh6Δ* subclones described in S2B Fig.
6	Ploidy measurements of strains isolated by same sex mating between T1 *pol2-4 msh6Δ* cultures described in S3 Fig.
7	Ploidy measurements of competition experiment between *pol2-4 msh6Δ* derived diploid and tetraploid strains described in Fig 2B.
8	Simulation of evolution of *pol3-01/pol3-01 msh6Δ/msh6Δ* evolved cultures described in S4 Fig.
9	Ploidy measurements of *pol3-01/pol3-01 msh6Δ/msh6Δ* evolved cultures described in Fig 3B.
10	Ploidy measurments of T25 *pol3-01/pol3-01 msh6Δ/msh6Δ* subclones analyzed in Fig 4
11	Mutation rate measurements of T25 *pol3-01/pol3-01 msh6Δ/msh6Δ* subclones described in Fig 4.

627

S2 Dataset. Whole genome sequencing of *pol3-01/pol3-01 msh6Δ/msh6Δ* strains.

Page	***Description***
AH164_B1_SNPs	Sequencing coverage, evolutionary relationships, distribution of variant allele frequencies (VAF), and annotation of SNPs for AH164_B1 subclones.
AH164_B1_Indels	Sequencing coverage, evolutionary relationships, distribution of VAFs, and annotation of Indels for AH164_B1 subclones.
AH164_B2_SNPs	Sequencing coverage, evolutionary relationships, distribution of VAFs, and annotation of SNPs for AH164_B2 subclones.

AH164_B2_Indels	Sequencing coverage, evolutionary relationships, distribution of VAFs, and annotation of Indels for AH164_B2 subclones.
AH164_C2_SNPs	Sequencing coverage, evolutionary relationships, distribution of VAFs, and annotation of SNPs for AH164_C2 subclones.
AH164_C2_Indels	Sequencing coverage, evolutionary relationships, distribution of VAFs, and annotation of Indels for AH164_C2 subclones.
AH164_D2_SNPs	Sequencing coverage, evolutionary relationships, distribution of VAFs, and annotation of SNPs for AH164_D2 subclones.
AH164_D2_Indels	Sequencing coverage, evolutionary relationships, distribution of VAFs, and annotation of Indels for AH164_D2 subclones.
AH164_G5_SNPs	Sequencing coverage, evolutionary relationships, distribution of VAFs, and annotation of SNPs for AH164_G5 subclones.
AH164_G5_Indels	Sequencing coverage, evolutionary relationships, distribution of VAFs, and annotation of Indels for AH164_G5 subclones.
AH164_A6_SNPs	Sequencing coverage, evolutionary relationships, distribution of VAFs, and annotation of SNPs for AH164_A6 subclones.
AH164_A6_Indels	Sequencing coverage, evolutionary relationships, distribution of VAFs, and annotation of Indels for AH164_A6 subclones.
AH164_B6_SNPs	Sequencing coverage, evolutionary relationships, distribution of VAFs, and annotation of SNPs for AH164_B6 subclones.
AH164_B6_Indels	Sequencing coverage, evolutionary relationships, distribution of VAFs, and annotation of Indels for AH164_B6 subclones.
AH164_C7_SNPs	Sequencing coverage, evolutionary relationships, distribution of VAFs, and annotation of SNPs for AH164_C7 subclones.
AH164_C7_Indels	Sequencing coverage, evolutionary relationships, distribution of VAFs, and annotation of Indels for AH164_C7 subclones.
Hypergeometric *p*-values	Tables of *p* values of hypergeometric tests of similarity between mutation spectra and multiple testing corrections.

628

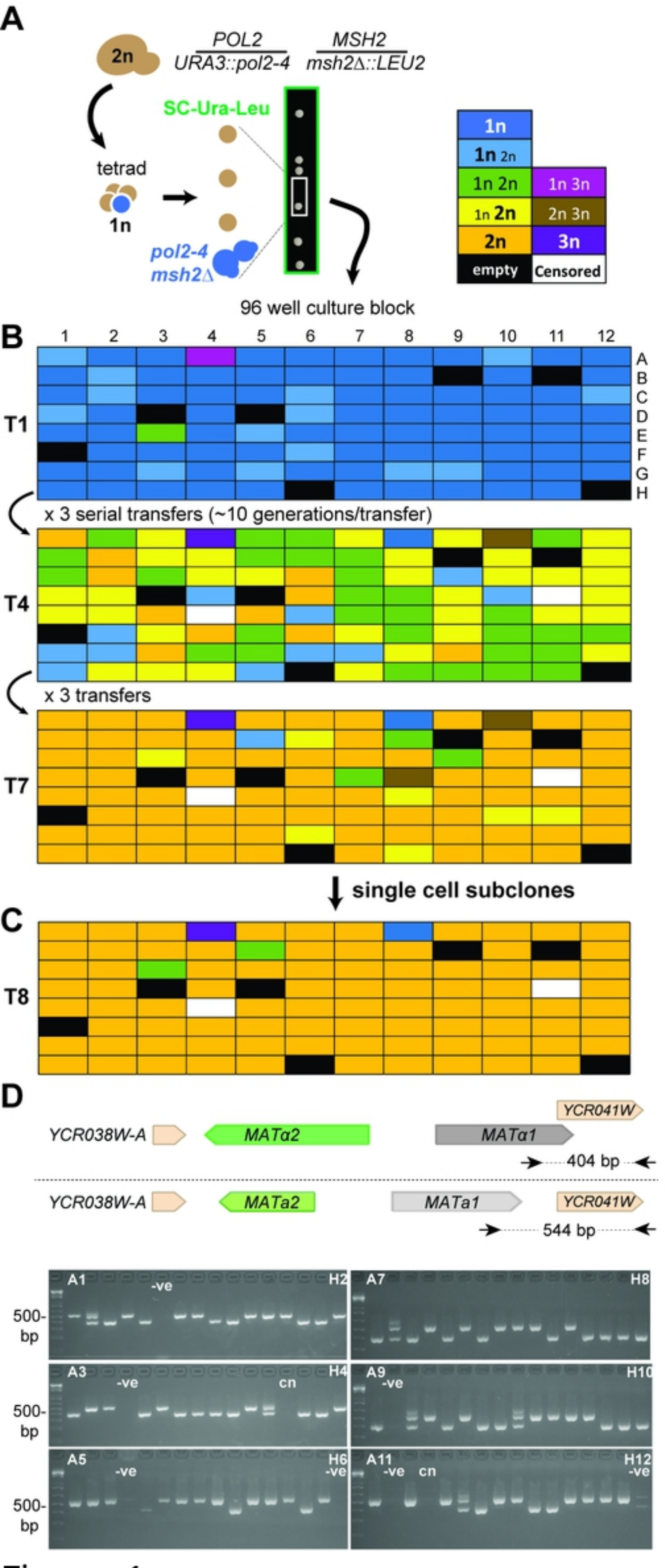
A
2n
POL2
URA3::pol2-4
MSH2
msh2Δ::LEU2
SC-Ura-Leu
tetrad
1n
pol2-4
msh2Δ
96 well culture block
1n
1n 2n
1n 2n
1n 3n
1n 2n
2n 3n
2n
3n
empty
Censored
B
1 2 3 4 5 6 7 8 9 10 11 12
A B C D E F G H
T1
x 3 serial transfers (~10 generations/transfer)
T4
x 3 transfers
T7
single cell subclones
C
T8
D
YCR041W
YCR038W-A
MATα2
MATα1
404 bp
YCR038W-A
MATa2
MATa1
YCR041W
544 bp
A1
-ve
H2
A7
H8
500-bp
A3
-ve
cn
H4
A9
-ve
H10
500-bp
A5
-ve
H6
-ve
A11
-ve
cn
H12
-ve
500-bp

Figure 1

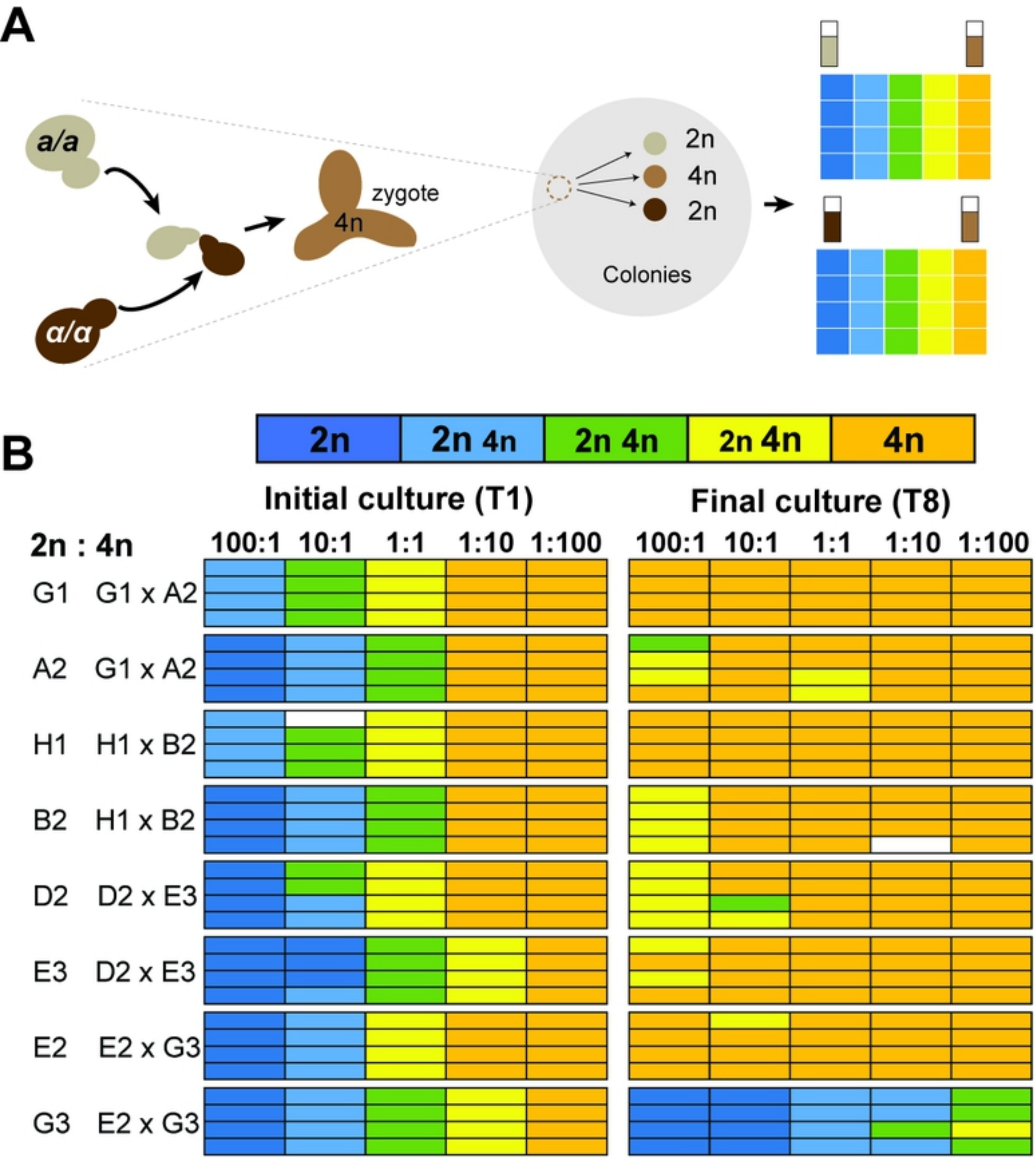
A
a/a
α/α
zygote
4n
2n
4n
2n
Colonies
B
2n
2n 4n
2n 4n
2n 4n
4n
Initial culture (T1)
Final culture (T8)
2n : 4n
100:1 10:1 1:1 1:10 1:100
100:1 10:1 1:1 1:10 1:100
G1 G1 x A2
A2 G1 x A2
H1 H1 x B2
B2 H1 x B2
D2 D2 x E3
E3 D2 x E3
E2 E2 x G3
G3 E2 x G3

Figure 2

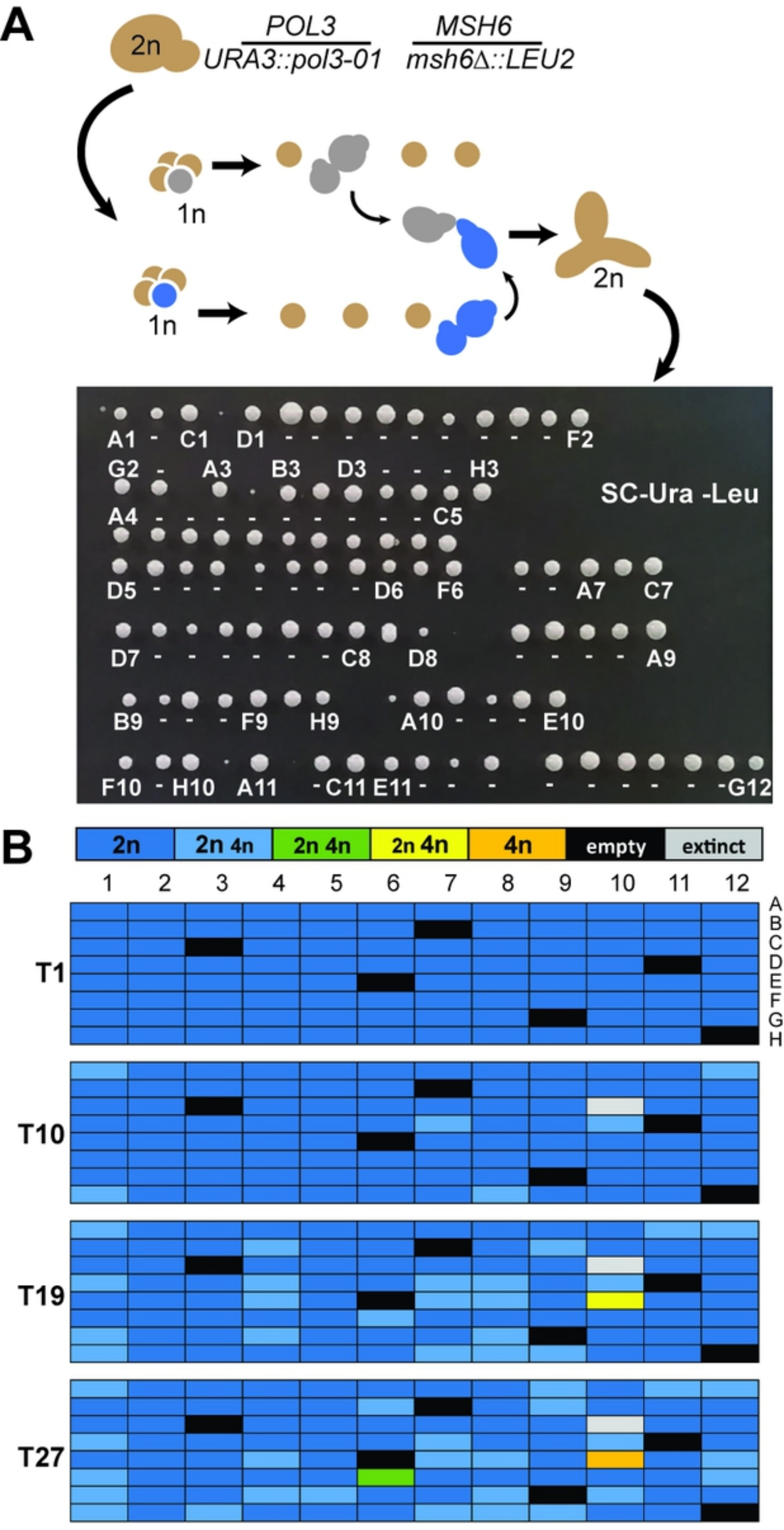
A
2n
POL3
URA3::pol3-01
MSH6
msh6Δ::LEU2
1n
1n
2n
SC-Ura -Leu
A1 C1 D1 F2
G2 A3 B3 D3 H3
A4 C5
D5 D6 F6 A7 C7
D7 C8 D8 A9
B9 F9 H9 A10 E10
F10 H10 A11 C11 E11 G12
B
2n
2n 4n
2n 4n
2n 4n
4n
empty
extinct
1 2 3 4 5 6 7 8 9 10 11 12
A B C D E F G H
T1
T10
T19
T27

Figure 3

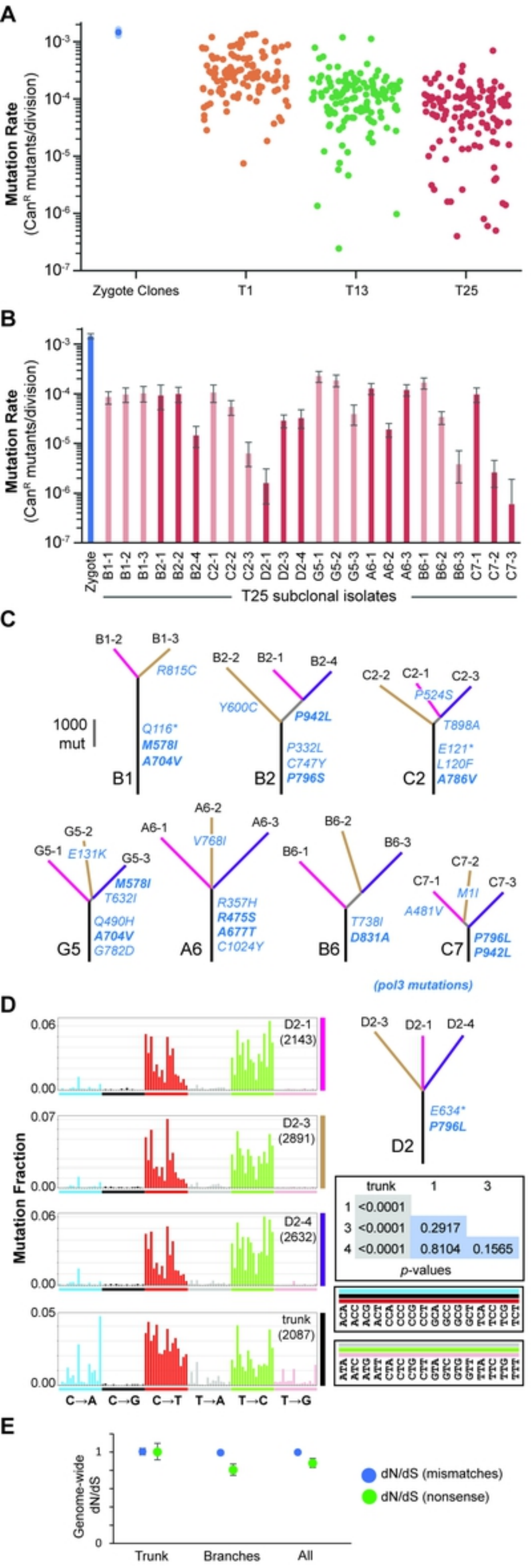
A
Mutation Rate
(CanR mutants/division)
Zygote Clones
T1
T13
T25
B
Zygote
T25 subclonal isolates
C
B1-2
B1-3
R815C
Q116*
M578I
A704V
B1
B2-2
B2-1
B2-4
Y600C
P942L
P332L
C747Y
P796S
B2
C2-2
C2-1
C2-3
P524S
T898A
E121*
L120F
A786V
C2
1000 mut
G5-1
G5-2
G5-3
E131K
M578I
T632I
Q490H
A704V
G782D
G5
A6-1
A6-2
A6-3
V768I
R357H
R475S
A677T
C1024Y
A6
B6-1
B6-2
B6-3
T738I
D831A
B6
C7-1
C7-2
C7-3
M1I
A481V
P796L
P942L
C7
(pol3 mutations)
D
Mutation Fraction
D2-1 (2143)
D2-3 (2891)
D2-4 (2632)
trunk (2087)
C→A
C→G
C→T
T→A
T→C
T→G
D2-3
D2-1
D2-4
E634*
P796L
D2
trunk 1 3
1 <0.0001
3 <0.0001 0.2917
4 <0.0001 0.8104 0.1565
p-values
E
Genome-wide dN/dS
Trunk
Branches
All
dN/dS (mismatches)
dN/dS (nonsense)

Figure 4

S1 Fig

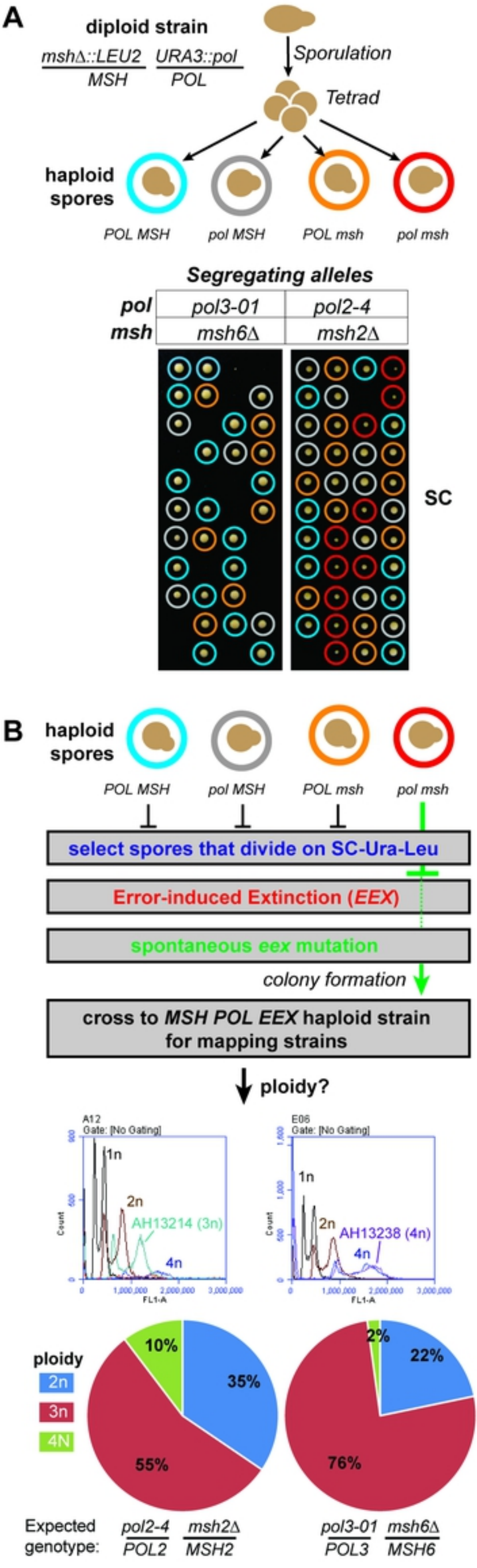

Supplementary Figure

S2 Fig.

A

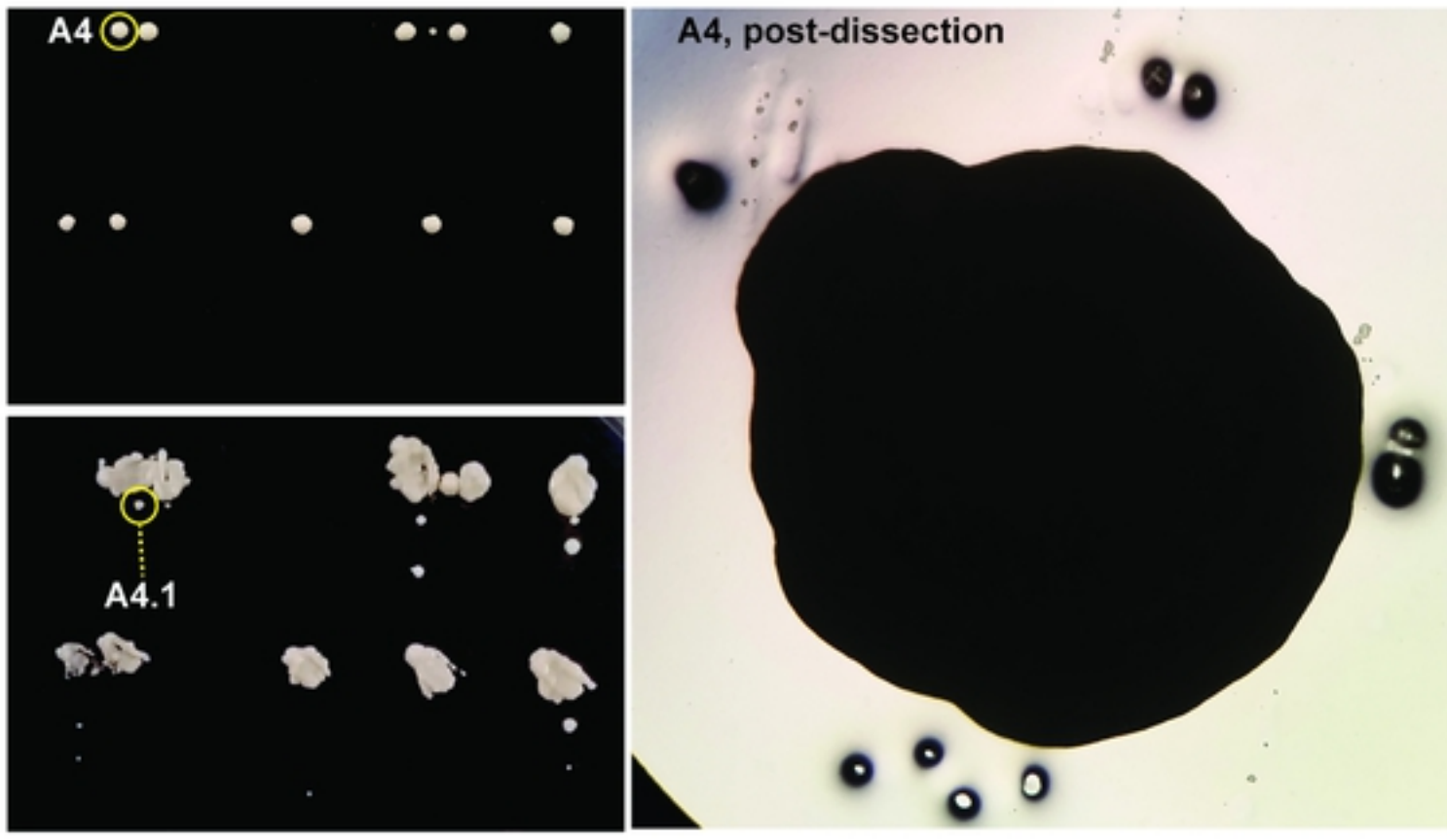

B

A1.3	G1.4	F2.1	B3.3	B4.3	E5.4	C6.4	G6.1	D7.3	B8.2	G8.4	D9.1
B1.1	A2.3	F2.2	E3.1	D4.4	G5.1	D6.1	G6.2	E7.3	B8.3	H8.1	H9.2
B1.2	B2.2	F2.4	E3.2	F4.2	G5.3	D6.4	G6.3	E7.4	C8.2	H8.2	A10.1
B1.4	B2.3	H2.2	G3.1	F4.3	H5.4	E6.2	B7.1	F7.3	C8.3	H8.4	C10.3
C1.2	B2.4	H2.4	G3.3	G4.2	A6.1	F6.1	B7.2	G7.3	D8.3	A9.1	C10.4
C1.3	D2.1	A3.1	H3.1	H4.2	B6.3	F6.2	C7.2	H7.4	F8.2	A9.4	D10.1
D1.3	E2.1	A3.2	A4.1	H4.3	C6.2	F6.3	C7.3	A8.2	F8.4	C9.1	D10.3
E1.4	E2.2	B3.1	B4.1	B5.4	C6.3	F6.4	C7.4	A8.3	G8.3	C9.3	D10.4

F10.2	E11.4	D12.1
G10.1	F11.1	D12.3
H10.1	F11.3	D12.2
A11.3	G11.4	E12.3
A11.4	A12.3	E12.4
C11.3	A12.4	F12.3
D11.1	B12.1	F12.4
D11.2	B12.2	G12.1

1n
1n 2n
1n 2n
1n 2n
2n
3n
poor growth

C

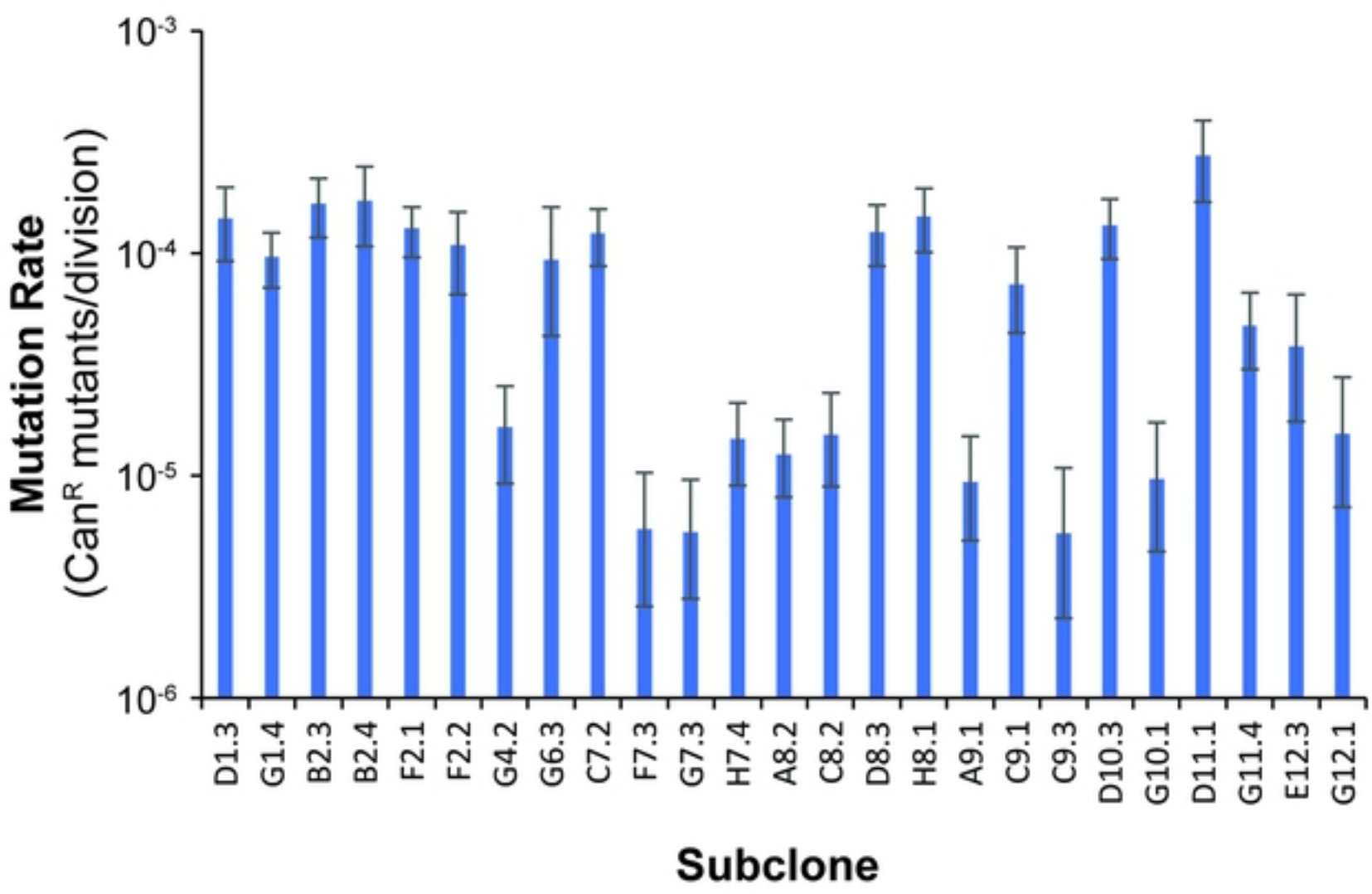

Supplementary Figure

S3 Fig.

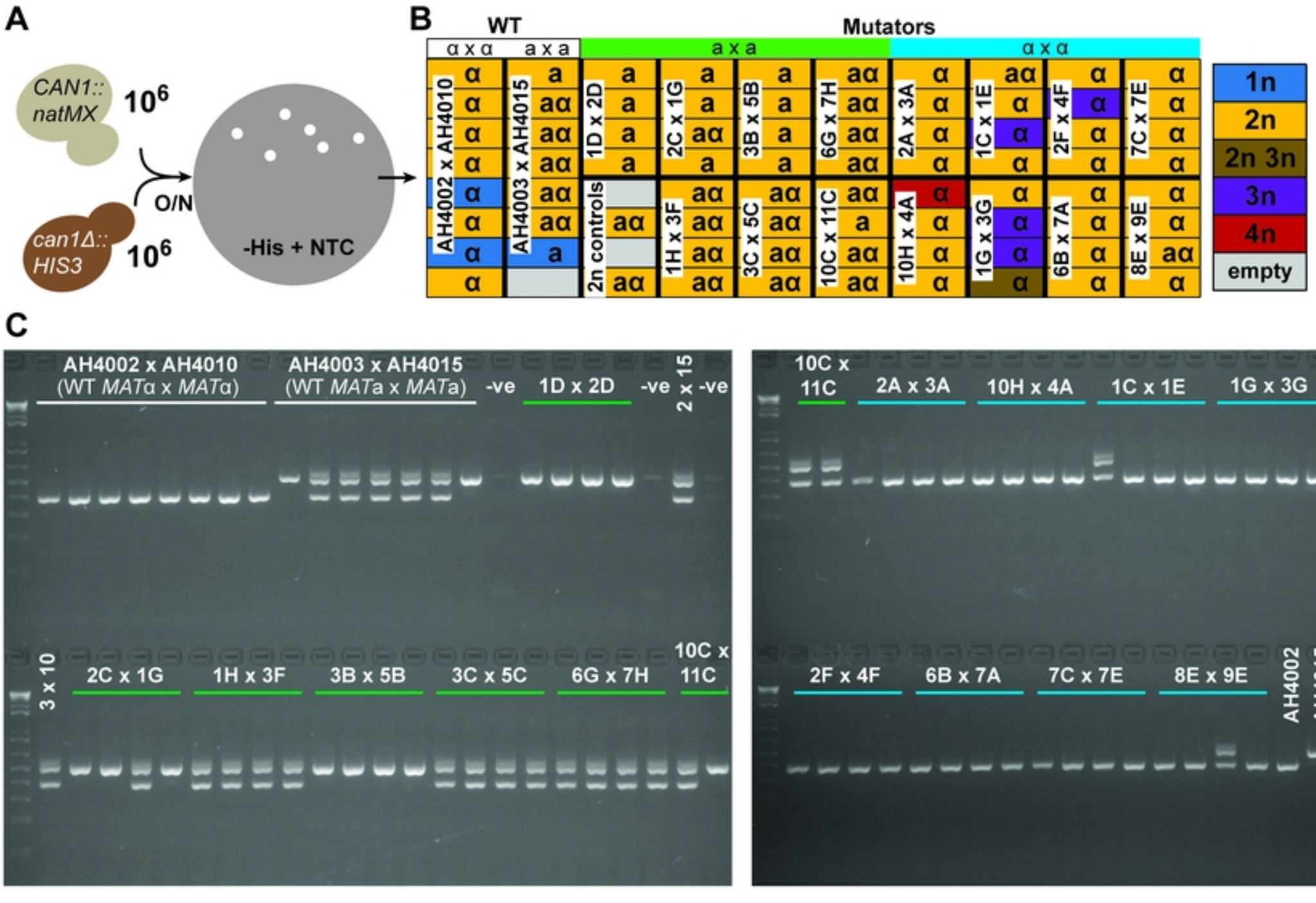

Supplementary Figure

S4 Fig.

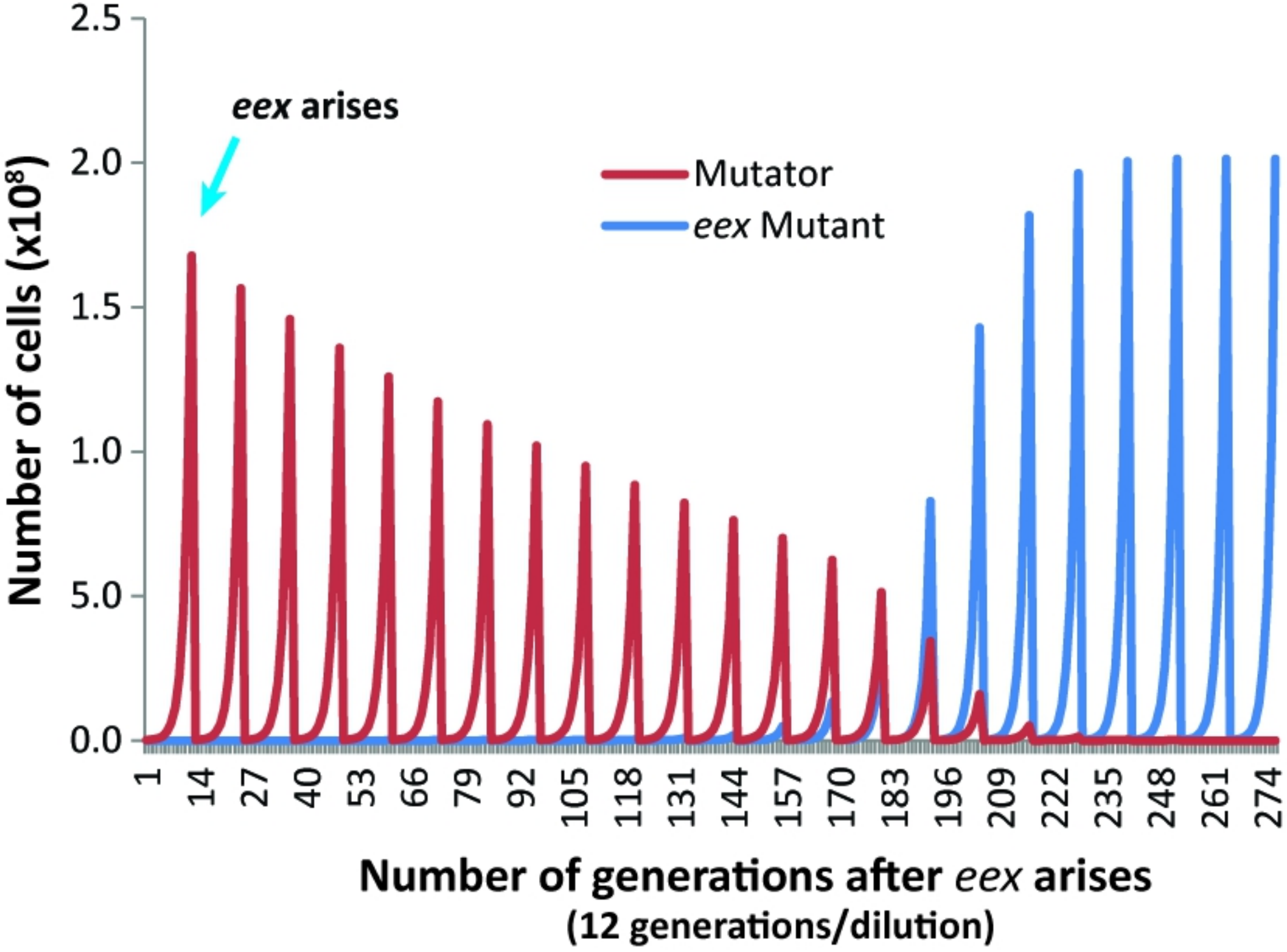

Supplementary Figure

S5 Fig.

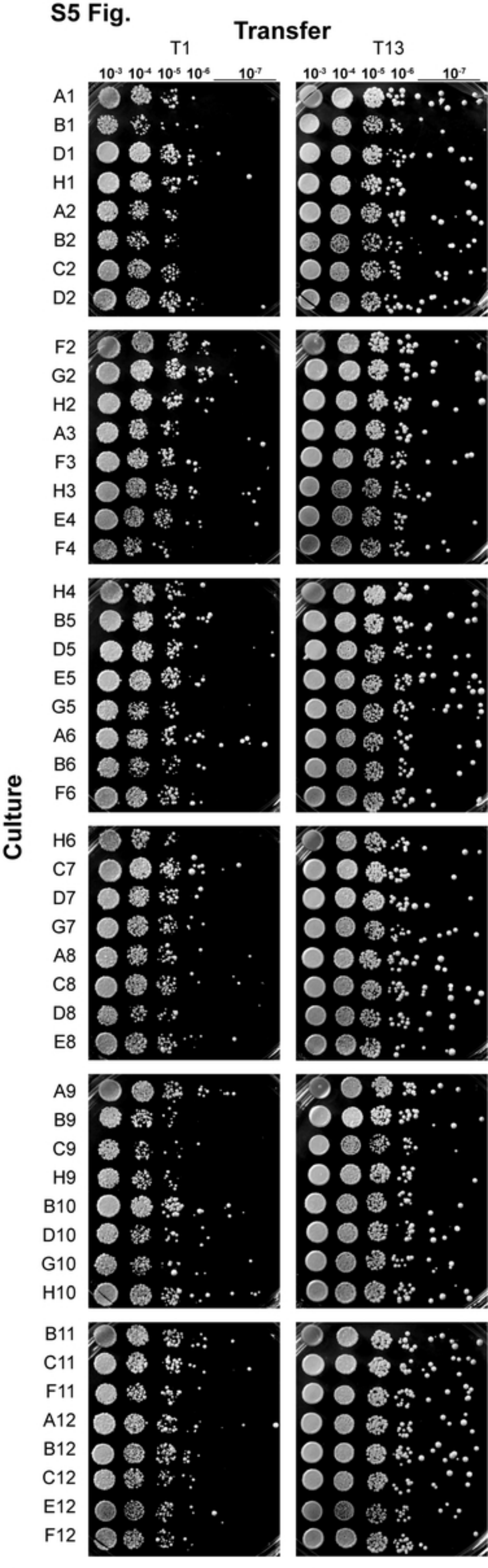

Supplementary Figure

S6 Fig.

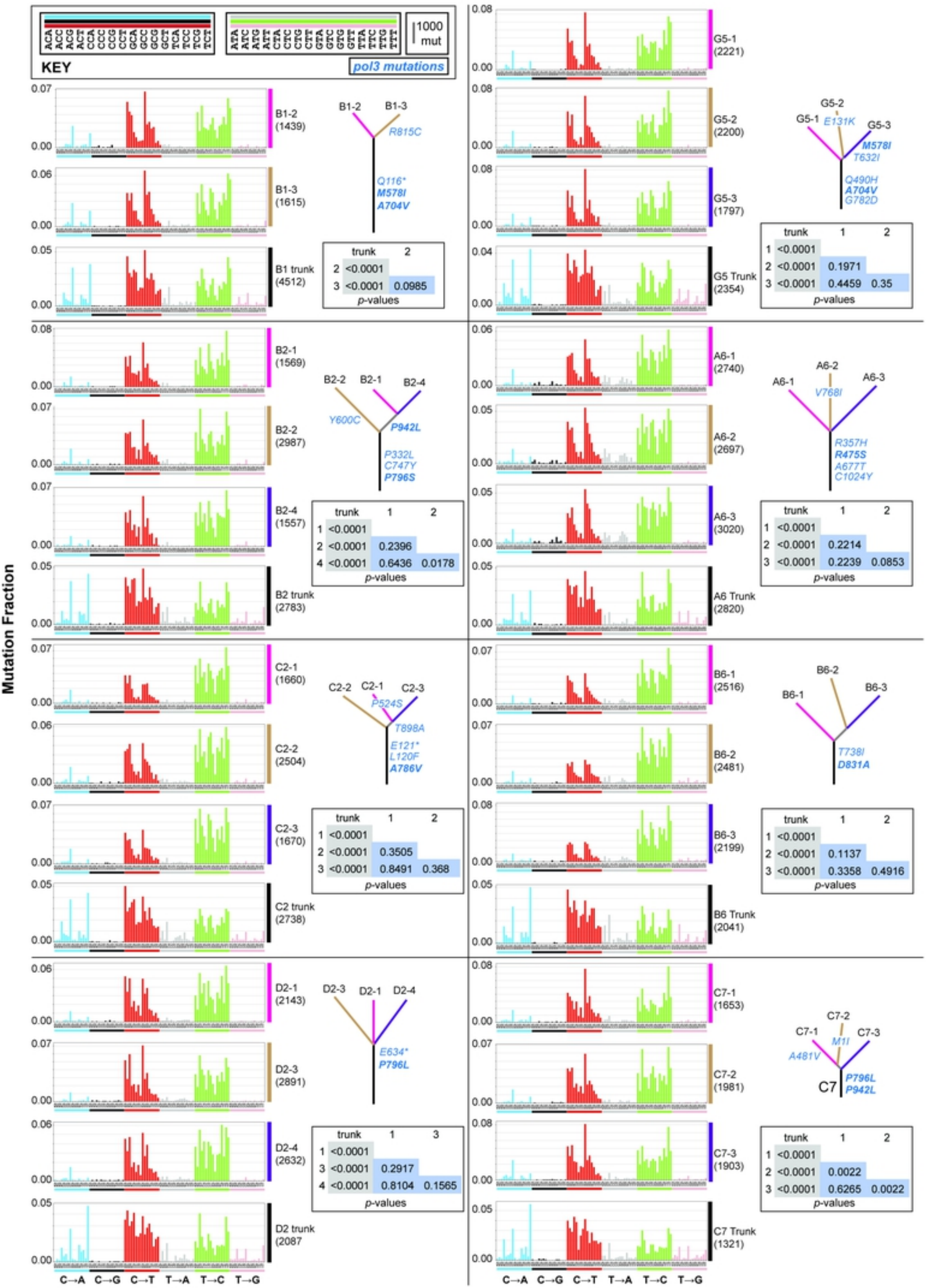

Supplementary Figure